How to cite: *Angew. Chem. Int. Ed.* **2023,** *62,* e202211663
International Edition: doi.org/10.1002/anie.202211663
German Edition: doi.org/10.1002/ange.202211663

Carbocatalysis

Catalytic Properties of High Nitrogen Content Carbonaceous Materials

*Enrico Lepre, Sylvain Rat, Cristian Cavedon, Peter H. Seeberger, Bartholomäus Pieber, Markus Antonietti, and Nieves López-Salas**

Abstract: The influence of structural modifications on the catalytic activity of carbon materials is poorly understood. A collection of carbonaceous materials with different pore networks and high nitrogen content was characterized and used to catalyze four reactions to deduce structure–activity relationships. The CO_2 cycloaddition and Knoevenagel reaction depend on Lewis basic sites (electron-rich nitrogen species). The absence of large conjugated carbon domains resulting from the introduction of large amounts of nitrogen in the carbon network is responsible for poor redox activity, as observed through the catalytic reduction of nitrobenzene with hydrazine and the catalytic oxidation of 3,3′,5,5′-tetramethylbenzidine using hydroperoxide. The material with the highest activity towards Lewis acid catalysis (in the hydrolysis of (dimethoxymethyl)benzene to benzaldehyde) is the most effective for small molecule activation and presents the highest concentration of electron-poor nitrogen species.

Introduction

Carbon-based materials are cheap, high surface area supports for metal catalysts. Activated charcoal has been known for over a century to promote the aerobic oxidation of organic molecules, such as ethanol, in the gas phase.[1] Nanostructured materials, including graphene,[2] graphene oxide,[3] carbon nanotubes, and nanodots[4] act as acid/base catalysts and promote redox reactions ("Carbocatalysis").[1,5] Manipulating the electron density via heteroatom doping is among the most studied strategies to tune the catalytic properties of carbonaceous materials.[1,6] Nitrogen doping results in the withdrawal of electron density from adjacent carbon atoms.[7] A graphene monolayer with nitrogen atoms inserted in the carbon backbone was studied using scanning tunneling microscopy,[8] and Mulliken charges of nitrogen-doped carbon materials were calculated.[6a,9] While the numbers differ, a negative charge localized on nitrogen atoms (between −0.2 and −0.6) and a positive charge on adjacent carbon atoms (between +0.05 and +0.58) were found in all cases.

For catalytic applications, nitrogen atoms with low oxidation states act as Lewis base, while the adjacent carbon atoms have Lewis acidic character.[7b,10] Carbon atoms close to nitrogen are involved in activating small electron-rich molecules, such as hydrazine or hydrogen peroxide, for redox reactions. The reduction of nitrobenzenes to anilines with hydrazine is facilitated by nitrogen atoms due to improved substrate adsorption.[7d,11] The performance of N-doped carbonaceous materials as Lewis acid/base catalysts and catalytic redox reactions has not been comprehensively investigated to date to understand the parameters that influence the catalytic activity of such materials.

Preparation of nitrogen-containing carbonaceous networks relies on nitrogen-containing carbon precursors or post-treatment of carbon materials with nitrogen-rich molecules. The resulting materials typically have low nitrogen content (<10 wt%), which limits the effect of heteroatom doping on the catalytic activity. Here, we present the preparation and characterization of nitrogen-rich nanocarbons from cytosine at different temperatures via a scalable and cost-efficient salt melt template synthesis. The catalytic activity in acid-, base- and redox catalysis was evaluated and compared with the properties of the carbonaceous materials.

Results and Discussion

A set of materials was synthesized from cytosine at different temperatures (500 °C, 600 °C, 700 °C, and 800 °C) using a salt melt (LiCl, $ZnCl_2$) template synthesis that promotes the formation of a porous network (Figure 1a).[12] In all cases, a mixture of LiCl, $ZnCl_2$, and cytosine (10:10:1 wt/wt/wt ratio) was heated to the target temperature at a heating ramp of 1 °C/min. After cooling to room temperature, the materials were washed with hydrochloric acid (0.1 M) to remove the salt template and obtain the nitrogen-rich

[*] E. Lepre, Dr. S. Rat, Prof. M. Antonietti, Dr. N. López-Salas
Department of Colloid Chemistry, Max Planck Institute of Colloids and Interfaces, Potsdam Science Park
Am Mühlenberg 1, 14476 Potsdam (Germany)
E-mail: nieves.lopezsalas@mpikg.mpg.de
Dr. C. Cavedon, Prof. P. H. Seeberger, Dr. B. Pieber
Department of Biomolecular Systems, Max Planck Institute of Colloids and Interfaces, Potsdam Science Park
Am Mühlenberg 1, 14476 Potsdam (Germany)

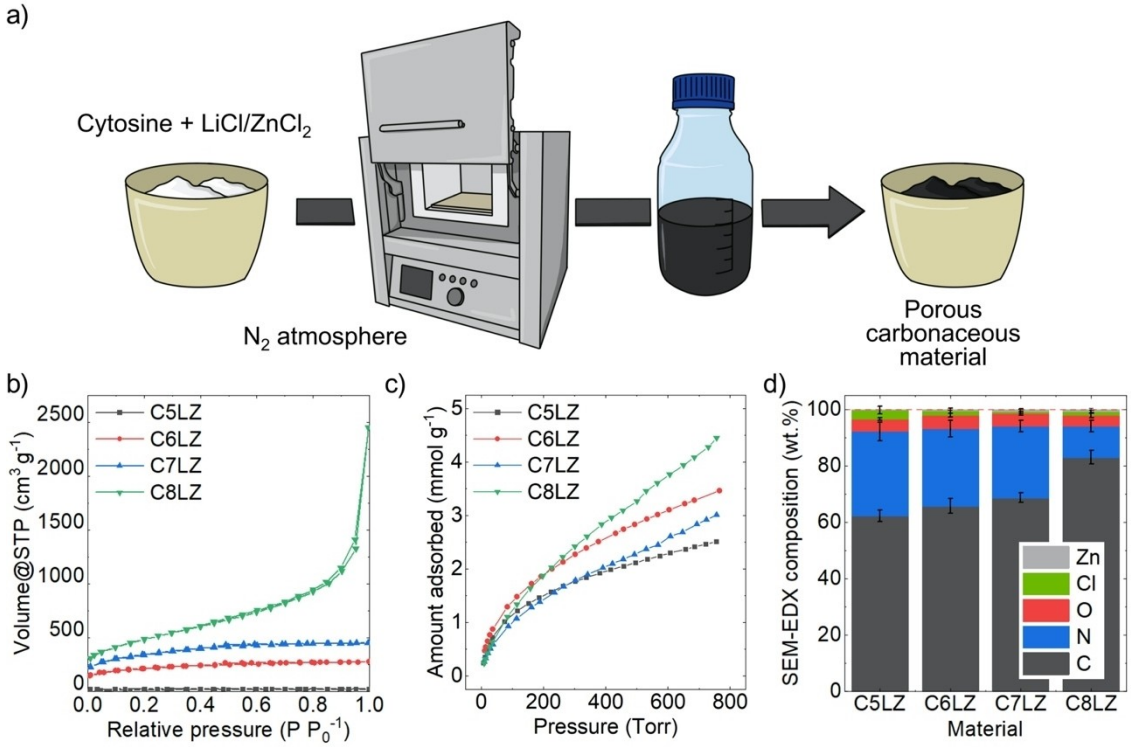

Figure 1. a) Synthesis of nitrogen-rich carbonaceous materials from cytosine in a LiCl/ZnCl$_2$ melt; b) N_2 adsorption-desorption isotherms at 77 K, c) CO_2 adsorption isotherm at 273 K, and d) SEM-EDX composition of the prepared samples.

carbon materials **C5LZ** (prepared from **c**ytosine at **5**00 °C in a **L**iCl/**Z**nCl$_2$ melt), **C6LZ**, **C7LZ**, and **C8LZ**.

The pore structure of the materials was analyzed by N_2 adsorption/desorption isotherms at 77 K (Figure 1b). The nitrogen isotherm shape of **C8LZ** indicates a hierarchical pore structure comprising micro-, meso-, and macropores.[13] **C7LZ** and **C6LZ** showed a sharp increase in the volume adsorbed at low relative pressures, characteristic of materials that have mainly a microporous structure. In addition, the small hysteresis loop at 0.5 P/P$_0$ in the nitrogen isotherms indicated a small fraction of mesopores. **C5LZ** showed poor nitrogen sorption, which is rationalized by the absence of a porous network.[7b] Specific surface areas were calculated by applying the Brunauer–Emmett–Teller (BET) equation to the adsorption branch of nitrogen adsorption isotherms and gave 44, 749, 1207, and 1701 $m^2 g^{-1}$ for **C5LZ**, **C6LZ**, **C7LZ**, and **C8LZ**, respectively (Table S1). Pore size distribution, calculated using quenched solid density functional theory (QSDT), confirmed these observations (Figure S1). While N_2 adsorption increases linearly with carbonization temperature, CO_2 adsorption isotherms recorded at 273 K showed a different trend (Figure 1c). The highest pore volume was calculated for **C8LZ** (0.180 $cm^3 g^{-1}$), and the lowest value was obtained for **C5LZ** (0.103 $cm^3 g^{-1}$). The pore volume calculated from CO_2 sorption for **C5LZ** is higher than the pore volume observed by N_2 sorption (Table S1), indicating a higher affinity for CO_2 binding due to its large nitrogen content. Despite its lower micropore volume, **C6LZ** had a higher CO_2 uptake than **C7LZ**. This is indicative of a higher affinity of carbon dioxide to the surface of **C6LZ**. Such an increase in affinity is typically ascribed to the presence of more pyridinic nitrogen functionalities.[14] These differences motivated the textural and chemical characterization of the samples.

Scanning electron microscopy (SEM) revealed that the materials present a texture formed by colloidal particles (Figure S2). This morphology indicates that the LiCl/ZnCl$_2$ mixture melts before condensation of the carbonaceous precursor starts such that the carbonaceous precursor dissolves in the ionic melt. Upon further heating, the carbon precursor condenses and precipitates as oligomer seeds, similar to a sol-gel mechanism. At higher temperatures, the seeds grow and form colloidal carbonaceous particles. A similar effect was observed in the salt melt template synthesis of carbon materials using ZnCl$_2$.[15] Transmission electron microscopy (TEM) confirmed that lower target temperatures result in less porous materials (Figure S3). A dense solid phase was observed for **C5LZ**, while increasing the target temperature results in more porous materials. Powder X-ray diffraction (XRD) analysis showed a broad band at 26.5° for **C5LZ** and **C6LZ**, which indicates layer stacking (Figure S4a). This signal was not observed for **C7LZ** and **C8LZ**, suggesting that de-stacking occurs at higher temperatures typical for highly porous materials. The tendency of the diffraction feature at 26.5° to widen into a weak broad band at 2θ ≈25–26° is characteristic of disordered frameworks.[16] Moreover, the development of large pore volumes fosters an increase in intensity at diffraction angles below 10°. On the contrary, when cytosine is directly carbonized in the presence of no salt melt at

different temperatures (samples **C5d**, **C6d**, **C7d**, and **C8d**), the peak at 26° increases with the increase of the carbonization temperature and the increase in the intensity at angles below 10° is not as intense (Figure S4b).

Composition analysis via energy-dispersive X-ray spectroscopy (SEM-EDX) (Figure 1d, Table S2) showed that the carbon content increases from 62.2 wt% to 83.0 wt% with increasing target temperature. In contrast, the nitrogen content decreases from 29.9 wt% to 11.1 wt%. This translates to an increase in the C/N ratio from 2.4 (**C5LZ**) to 8.7 (**C8LZ**) (Figure S5). The oxygen content slightly varies from 4.8 wt% to 3.8 wt%. Here it is important to mention that, to avoid the overestimation of the oxygen content of the samples, each material was degassed at 150 °C in a vacuum oven for 12 h to remove the contribution of weakly bonded water molecules.[17] All materials contain small amounts of chlorine (0.3–3.2 wt%) and zinc (0.1–0.3 wt%) that originate from the salt melt template synthesis, which was further confirmed by inductively coupled plasma analysis (ICP) (Table S3).

X-ray photoelectron spectroscopy (XPS) was used to investigate the chemical structure of all materials in detail (Figure S6). The deconvoluted high-resolution N1s XPS spectrum showed peaks centered at 398 eV, 400 eV, 401 eV, and 402 eV, which indicates that the materials contain nitrogen atoms with low ("electron-rich") and high ("electron-poor") oxidation states (Table S4, Figure S7). Even though the high nitrogen content and the amorphous nature of the materials renders difficult an assignment to specific functionalities, the conventional assignments will be used for clarity purposes. The peaks at 398 eV, 400 eV, 401 eV, and 402 eV will be ascribed to pyridinic, pyrrolic, quaternary, and N-oxide nitrogen atoms, respectively.[7c,18] Because the materials significantly differ in their total nitrogen content, the amount of each nitrogen species was calculated in mol per 100 g of material for better comparison using the data obtained from SEM-EDX and XPS experiments (Figure 2a). A slightly higher amount of nitrogen atoms with high oxidation states (i.e., quaternary nitrogen at 401 eV and 402 eV) was observed for **C6LZ** compared to **C5LZ** and stayed almost constant at higher synthesis temperatures. It is worth noting that these nitrogen species still carry a negative Mulliken charge even though they present a high oxidation state.[9] On the contrary, the number of nitrogen atoms with low oxidation states (i.e., pyridinic and pyrrolic) decreases gradually with rising target temperatures.

The deconvoluted spectra of the C1s peak showed three bands centered at 284 eV, 286 eV, and 288 eV (Figure 2b, Figure S6). This relates to carbon atoms with low (sp^2 C–C bonds, 284 eV) and high (bound to one or more heteroatoms, 286 eV and 288 eV) oxidation states. Although the total carbon content increases at higher target temperatures, the amount of carbon atoms at 284 eV remains similar for **C5LZ**, **C6LZ**, and **C7LZ** (Table S5, Figure 2b). The deconvolution peaks centered at 286 eV and 288 eV indicated an increase of electron-poor carbon atoms from **C5LZ** (1.6 mol/100 g) to **C7LZ** (2.3 mol/100 g). **C8LZ** showed significant differences compared to other materials. The total amount of carbons with high oxidation states (286 eV and 288 eV) is low (1.5 mol/100 g), whereas a comparably high amount of carbons at 284 eV was calculated (5.4 mol/100 g). This observation agrees with the high total carbon content for **C8LZ**, which translates to more C–C bonds in the material. The deconvoluted spectra of the O1s peak showed that the proportion of C=O and C–O–C groups does not change significantly by increasing the temperature (the C=O/C–O–C area ratio 1:0.60 ± 0.02 is for all the samples). Taking into account the very steady amount of oxygen in the samples, we will not consider oxygen contributions as a possible factor influencing the catalytic performance of these samples.

Temperature-programmed desorption (TPD) was used to study the interaction of ammonia with all materials (Figure 2c). **C8LZ** had a desorption band with low intensity from 100 °C up to 250 °C. From **C5LZ** to **C7LZ**, the desorption band became sharper and more intense, and the desorption maximum shifted to lower temperatures. The higher intensity of the NH_3-TPD traces can be rationalized by a higher amount or better accessibility of Lewis acidic groups, and the desorption maximum at lower temperatures indicates a lower Lewis acidity. The uptrend observed for C8LZ is ascribed to ammonia slowly desorbing from its

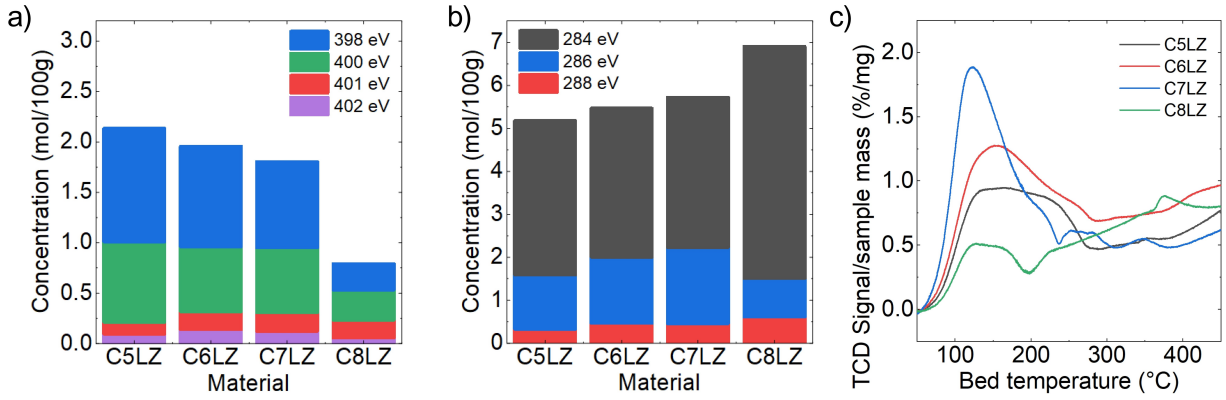

Figure 2. a) Concentration (mol/100 g) of nitrogen species as obtained from N1s XPS and SEM-EDX composition, b) concentration (mol/100 g) of carbon species as obtained from C1s XPS and SEM-EDX composition, and c) NH_3-TPD profile of C5LZ, C6LZ, C7LZ, and C8LZ.

much larger pore volume as TPD traces of the sample prior to ammonia adsorption, and TGA analysis in nitrogen atmosphere shows that that the sample is stable in that temperature range (Figure S8).

Correlating properties of nitrogen-doped carbonaceous materials with catalytic activity is challenging because varying the amount of nitrogen is accompanied by other changes, such as a different surface area and pore size distribution. We decided to investigate the structure–activity relationship of all materials for four different reactions to study the influence of each parameter. The catalytic reduction of nitrobenzene in the presence of hydrazine (N_2H_4) and the catalytic oxidation of 3,3′,5,5′-tetramethylbenzidine (TMB) using hydrogen peroxide (H_2O_2) were chosen as model reactions to study the factors influencing the activation of small, electron-rich molecules in redox reactions. The ability of the materials to serve as acid and base catalysts was studied for the synthesis of cyclic carbonates from CO_2 and epichlorohydrin (ECH), as well as the hydrolysis of (dimethoxymethyl)benzene (DMB) to benzaldehyde (BA) followed by a Knoevenagel reaction with malononitrile in a one-pot two-step procedure.

First, we studied the catalytic reduction of nitrobenzene with N_2H_4 at room temperature using a reaction time of 48 h (Figure 3a). It was previously proposed that carbon materials catalyze this reaction by creating a pool of electrons through the adsorption of hydrazine[19] and that the catalyst activity can be improved by tailoring the adsorption energy by nitrogen and sulfur doping.[20] In addition, in 2018, nitrogen doping was shown by Chanjuan Liao et al. as an effective strategy to generate active sites for reductions in the presence of hydrazine.[21] Accordingly to these results, the desired product was obtained in excellent yield when **C8LZ** was used. Nonetheless, a small amount of the desired product was detected in the case of **C7LZ**, While **C6LZ** and **C5LZ** did not yield in the formation of aniline.

Next, the catalytic activity of the materials was evaluated for the oxidation of TMB with hydrogen peroxide by tracking the reaction progress using UV/Vis spectroscopy (Figure 3b, Figure S9). Similar to the results obtained for the nitro reduction described above, **C8LZ** had the highest catalytic activity. The use of **C7LZ** resulted in a moderate yield of the oxidation product. **C5LZ** and **C6LZ** showed almost no catalytic activity. The reaction using **C8LZ** was analyzed using Michaelis–Menten kinetics (Figure S10, Table S7).[22] The maximum rate at a saturating substrate concentration (V_{max}) was 0.8 $\mu M s^{-1}$. The substrate concentration at which the reaction rate is half of v_{max} (K_M) was 28.0 mM. A comparison with previously published carbonaceous materials as catalysts for the same transformations shows that **C8LZ** presents the highest v_{max} and the second-highest K_M reported to date (Table S7).[23,24]

Due to the low catalytic activity of **C5LZ**, **C6LZ**, and **C7LZ** in both reactions, few conclusions can be drawn. Although electron-poor carbons are, to a certain degree, responsible for the adsorption of small molecules, their amount and Lewis acidity is likely not the critical parameter to promote these reactions. The catalytic activity of **C5LZ**, **C6LZ**, and **C7LZ**, which contain many electron-poor carbon atoms in their carbon network, was low. A large surface area and extensive pore structure do not guarantee high catalytic performance. **C6LZ** presents a larger surface area than previously reported nitrogen-doped carbonaceous materials, but its catalytic activity in both model reactions was low.[23] Only when the surface area is increased over 1000 $m^2 g^{-1}$ does the effect of the extensive pore network affect the catalytic activity (see the performance of sample C7LZ). Here, it is important to point out that oxygen functionalities might also act as active sites as described by

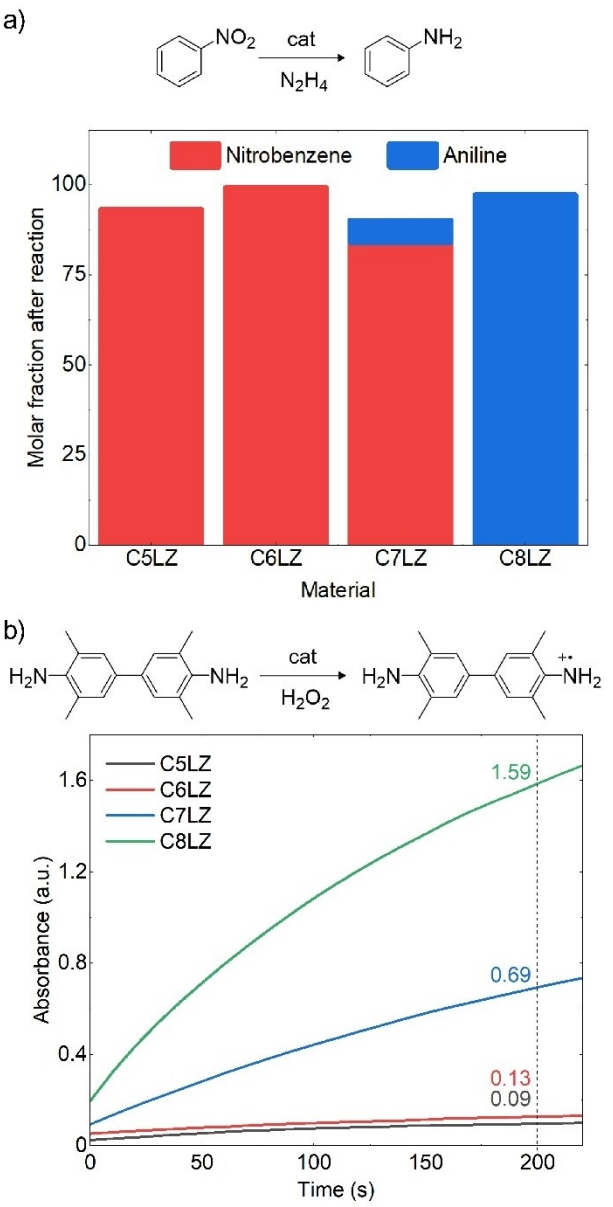

Figure 3. a) Catalytic reduction of nitrobenzene in the presence of hydrazine (N_2H_4) and molar fraction of aniline and nitrobenzene after 48 h obtained by ^{1}H NMR (5 mg catalyst, ethanol as solvent, and $N_2H_4 \cdot H_2O$). b) Catalytic oxidation of 3,3′,5,5′-tetramethylbenzidine (TMB) using hydrogen peroxide (H_2O_2).The kinetic profile was determined via the absorbance at 652 nm (5μg L^{-1} of catalyst, 0.25 mM of TMB, 40 mM H_2O_2, and 1 mL water).

Shuchang Wu et al.[25] However, the rather constant oxygen content in the different samples suggests that they might not be the main catalytic active site of the samples.

The fact that **C5LZ**, **C6LZ**, and **C7LZ** do not show high catalytic activity suggests that a very high nitrogen content is detrimental for redox catalysis, likely because it lowers the dimension of conjugated carbon domains. These domains are critical for electron transfer processes.[26] The high K_M of **C8LZ** in the TMB oxidation indicates that a high H_2O_2 concentration is necessary to saturate the catalytically active sites. Other studies using carbon-based materials show that K_M decreases upon nitrogen doping, rationalized by a higher affinity to H_2O_2.[23a,24b] We assume that the high nitrogen content in **C8LZ**, in combination with the porous morphology, results in a situation where catalytically active sites are accessible but slowly saturated.

We studied the ability of high nitrogen-content carbonaceous materials to serve as catalysts in the synthesis of cyclic carbonates from CO_2 and epichlorohydrin at 130 °C (Figure 4a, Table S8). The use of **C6LZ** resulted in the highest conversion (58 %) of epichlorohydrin, but the selectivity towards the desired product was only moderate (61 %). No side products were detected using ^{1}H NMR analysis (Figure S11), suggesting that polymerization reactions are responsible for the low selectivity.[27] A lower conversion (27 %) but excellent selectivity (95 %) was observed for **C8LZ**. **C7LZ** showed low activity (36 % conversion) and selectivity (46 %). The use of **C5LZ** did not result in any reaction of ECH. This reaction requires the activation of CO_2 with a nucleophile (Lewis base).[28] Consequently, the results confirm the presence of Lewis basic sites within the structure of **C6LZ**, **C7LZ**, and **C8LZ**. According to the accepted mechanism, a Lewis acid is not required but can improve carbonate formation.[28] Our results suggest that **C6LZ** (highest ECH conversion) and **C8LZ** (highest selectivity) have the highest amount of Lewis acidic sites of all tested materials.

For an in-depth analysis, we studied the acid-catalyzed hydrolysis of (dimethoxymethyl)benzene (DMB) to benzaldehyde (BA) followed by a base-mediated Knoevenagel condensation that yields benzomalononitrile (BMN) (Figure 4b).[29] The two-step one-pot reaction was monitored by ^{1}H- NMR analysis (Figure S12, Figure S13). The amount of DMB that was consumed after one hour showed that **C8LZ** (80 % DMB conversion) is a better Lewis acid catalyst than **C7LZ** (65 % DMB conversion) and **C6LZ** (52 % DMB conversion) (Figure 4b). The base-catalyzed conversion of BA to BMN follows a negative trend for the same set of materials due to the decreasing Lewis basic sites from **C6LZ** to **C8LZ**. **C5LZ** shows good activity for Lewis acid catalysis but performs poorly as a Lewis base catalyst. Likely the low surface area of **C5LZ** is responsible for that finding. In the case of **C6LZ**, **C7LZ**, and **C8LZ**, the obtained results are in agreement with speciation via XPS analysis. The activity in Lewis base catalysis decreases in line with the decrease of electron-rich pyridinic and pyrrolic nitrogen atoms. In contrast, the activity towards Lewis acid catalysis increases with a higher amount of electron-poor carbon atoms. This is in agreement with our observation from NH_3-TPD. The

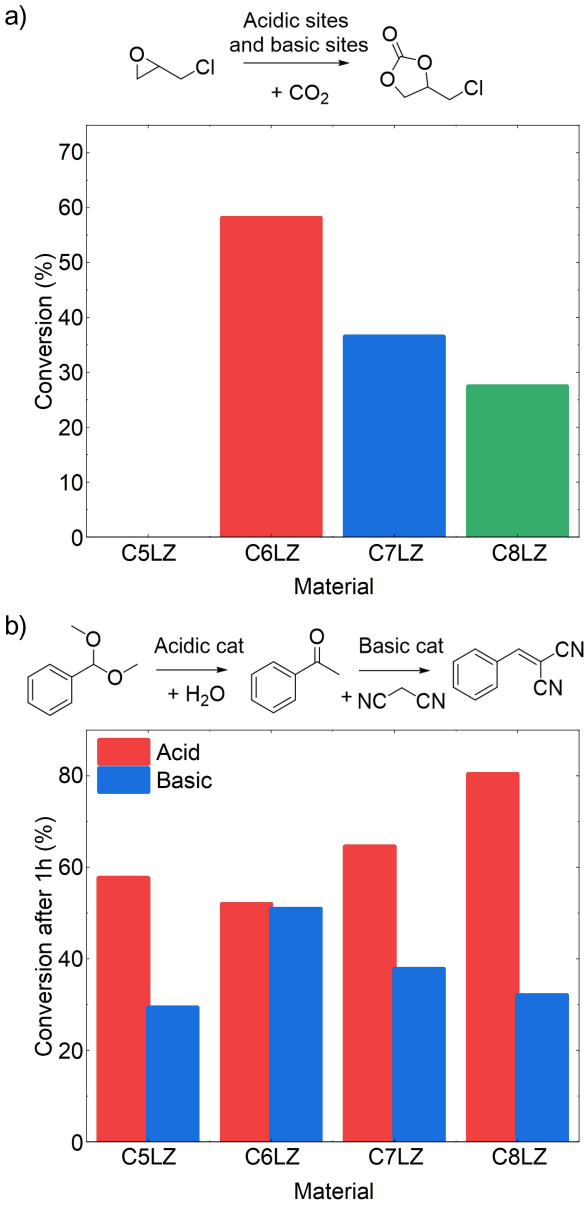

Figure 4. a) CO_2 cycloaddition to epichlorohydrin and conversion values obtained by ^{1}H NMR in the presence of an internal standard using the different materials as catalysts. b) Acid-catalyzed hydrolysis of (dimethoxymethyl)benzene (DMB) to benzaldehyde (BA) followed by a base-mediated Knoevenagel condensation and conversions for the acidic (red) and basic (blue) reaction as obtained by ^{1}H NMR in the presence of an internal standard using the different materials as catalysts.

samples showing larger amounts of electron-poor carbon atoms also have a higher ratio of electron-poor over electron-rich nitrogen atoms. These nitrogen electron-poor atoms can promote the formation of more positive charges on the adjacent carbon atoms.[9] These results confirm that strategic nitrogen doping tailors carbonaceous materials Lewis acidic and basic properties.

Our findings reveal that CO_2 and ECH reaction conversion follows a similar trend as the Knoevenagel reaction, indicating its dependence on Lewis basic sites. All materials show almost complete conversion in the two-step, one-pot

BA synthesis (Figure S12), confirming the absence of large conjugated carbon domains as the main factor in the low activity towards the activation of N_2H_4 and H_2O_2 of **C5LZ**, **C6LZ**, and **C7LZ**. The material with the highest Lewis acid catalysis activity (**C8LZ**) is also the most effective material for small molecule activation and presents the highest concentration of quaternary nitrogen. These are key structural features for Lewis acidity of nitrogen-doped carbon-based materials.

Conclusion

We present a simple, straightforward synthetic method for carbonaceous materials with high nitrogen content (up to 34 wt% nitrogen content) and a high surface area (up to 1701 $m^2 g^{-1}$). The materials were characterized by N_2 and CO_2 sorption, SEM-EDX, TEM, PXRD, XPS, and TPD to study the influence of the synthesis temperature on the surface area, composition, and surface electron density. The materials are active catalysts for the reduction of nitrobenzene with N_2H_4, the oxidation of 3,3′,5,5′-tetramethylbenzidine H_2O_2, the synthesis of cyclic carbonate from CO_2 and epichlorohydrin, and a two-step one-pot synthesis of benzomalononitrile that involves Lewis acid and Lewis base catalysis. Our results identified the critical physicochemical parameters of such materials for catalytic applications. N_2H_4 and H_2O_2 can be activated on the surface of nitrogen-doped carbonaceous materials through Lewis acidic sites. If the nitrogen content becomes too high, a detrimental effect was observed due to the loss of a conjugated structure. Cyclic carbonate synthesis mainly depended on Lewis basic sites identified that activate CO_2. The amount of electron-poor quaternary nitrogen atoms could be correlated to the activity in Lewis acid catalysis and was ascribed to the presence of electron-poor carbon atoms next to electron-poor nitrogen species.

Acknowledgements

The Max Planck Society is gratefully acknowledged for financial support. B.P. acknowledges financial support from the German Chemical Industry Fund (Fonds der Chemischen Industrie, FCI) through a Liebig Fellowship of. S.R. acknowledges the Alexander Von Humboldt Stiftung for a research fellowship. J. Brandt is gratefully acknowledged for the help provided during ICP analyses. A. Voelkel is gratefully acknowledged for the help provided with TGA analyses. Heike Runge and Bolortuya Badamdorj are gratefully acknowledged for the help provided with TEM, SEM, and SEM-EDX analysis. Open Access funding enabled and organized by Projekt DEAL.

Conflict of Interest

The authors declare no conflict of interest.

Data Availability Statement

The data that support the findings of this study are available from the corresponding author upon reasonable request.

Keywords: Acid/Base Catalysis · Carbocatalysis · Carbonaceous Materials · Nitrogen Doping · Redox Catalysis

[1] M. Antonietti, N. Lopez-Salas, A. Primo, *Adv. Mater.* **2019**, *31*, 1805719.
[2] S. Navalon, A. Dhakshinamoorthy, M. Alvaro, H. Garcia, *Chem. Rev.* **2014**, *114*, 6179–6212.
[3] C. Su, K. P. Loh, *Acc. Chem. Res.* **2013**, *46*, 2275–2285.
[4] C. Rosso, G. Filippini, M. Prato, *ACS Catal.* **2020**, *10*, 8090–8105.
[5] a) D. S. Su, S. Perathoner, G. Centi, *Chem. Rev.* **2013**, *113*, 5782–5816; b) P. Tang, G. Hu, M. Li, D. Ma, *ACS Catal.* **2016**, *6*, 6948–6958; c) D. S. Su, G. Wen, S. Wu, F. Peng, R. Schlögl, *Angew. Chem. Int. Ed.* **2017**, *56*, 936–964; *Angew. Chem.* **2017**, *129*, 956–985.
[6] a) X. Duan, K. O'Donnell, H. Sun, Y. Wang, S. Wang, *Small* **2015**, *11*, 3036–3044; b) X. Sun, B. Li, T. Liu, J. Song, D. S. Su, *Phys. Chem. Chem. Phys.* **2016**, *18*, 11120–11124.
[7] a) C. Yuan, W. Chen, L. Yan, *J. Mater. Chem.* **2012**, *22*, 7456–7460; b) J. Kossmann, T. Heil, M. Antonietti, N. Lopez-Salas, *ChemSusChem* **2020**, *13*, 6643–6650; c) R. Arrigo, M. Hävecker, S. Wrabetz, R. Blume, M. Lerch, J. McGregor, E. P. J. Parrott, J. A. Zeitler, L. F. Gladden, A. Knop-Gericke, R. Schlögl, D. S. Su, *J. Am. Chem. Soc.* **2010**, *132*, 9616–9630; d) Y. Gao, G. Hu, J. Zhong, Z. Shi, Y. Zhu, D. S. Su, J. Wang, X. Bao, D. Ma, *Angew. Chem. Int. Ed.* **2013**, *52*, 2109–2113; *Angew. Chem.* **2013**, *125*, 2163–2167; e) X.-K. Kong, Z.-Y. Sun, M. Chen, C.-L. Chen, Q.-W. Chen, *Energy Environ. Sci.* **2013**, *6*, 3260–3266; f) D.-W. Wang, D. Su, *Energy Environ. Sci.* **2014**, *7*, 576–591; g) D. Guo, R. Shibuya, C. Akiba, S. Saji, T. Kondo, J. Nakamura, *Science* **2016**, *351*, 361–365.
[8] L. Zhao, R. He, K. T. Rim, T. Schiros, K. S. Kim, H. Zhou, C. Gutierrez, S. P. Chockalingam, C. J. Arguello, L. Palova, D. Nordlund, M. S. Hybertsen, D. R. Reichman, T. F. Heinz, P. Kim, A. Pinczuk, G. W. Flynn, A. N. Pasupathy, *Science* **2011**, *333*, 999–1003.
[9] a) A. Legarreta-Mendoza, N. Flores-Holguín, D. Lardizabal-Gutiérrez, *Int. J. Hydrogen Energy* **2019**, *44*, 12374–12380; b) J. Gu, Q. Du, Y. Han, Z. He, W. Li, J. Zhang, *Phys. Chem. Chem. Phys.* **2014**, *16*, 25498–25507.
[10] J. Porwal, N. Karanwal, S. Kaul, S. L. Jain, *New J. Chem.* **2016**, *40*, 1547–1553.
[11] J. Xi, Q. Wang, J. Liu, L. Huan, Z. He, Y. Qiu, J. Zhang, C. Tang, J. Xiao, S. Wang, *J. Catal.* **2018**, *359*, 233–241.
[12] a) X. Liu, N. Fechler, M. Antonietti, *Chem. Soc. Rev.* **2013**, *42*, 8237–8265; b) N. Fechler, T.-P. Fellinger, M. Antonietti, *Adv. Mater.* **2013**, *25*, 75–79.
[13] a) M. Thommes, K. Kaneko, A. V. Neimark, J. P. Olivier, F. Rodriguez-Reinoso, J. Rouquerol, K. S. W. Sing, *Pure Appl. Chem.* **2015**, *87*, 1051–1069; b) S. M. G. Lama, J. Pampel, T.-P. Fellinger, V. P. Beškoski, L. Slavković-Beškoski, M. Antonietti, V. Molinari, *ACS Sustainable Chem. Eng.* **2017**, *5*, 2415–2420; c) J. Pampel, T.-P. Fellinger, *Adv. Energy Mater.* **2016**, *6*, 1502389.
[14] a) L. Wang, R. T. Yang, *J. Phys. Chem. C* **2012**, *116*, 1099–1106; b) J. Gong, H. Lin, M. Antonietti, J. Yuan, *J. Mater. Chem. A* **2016**, *4*, 7313–7321; c) J. Gong, H. Lin, K. Grygiel, J. Yuan, *Appl. Mater. Today* **2017**, *7*, 159–168; d) K. V. Kumar, K. Preuss, L. Lu, Z. X. Guo, M. M. Titirici, *J. Phys. Chem. C* **2015**, *119*, 22310–22321.

[15] N. Díez, A. B. Fuertes, M. Sevilla, *Energy Storage Mater.* **2021**, *38*, 50–69.
[16] a) M. Sevilla, G. A. Ferrero, N. Diez, A. B. Fuertes, *Carbon* **2018**, *131*, 193–200; b) M. Cox, R. Mokaya, *Sustainable Energy Fuels* **2017**, *1*, 1414–1424; c) F. Xu, Z. Tang, S. Huang, L. Chen, Y. Liang, W. Mai, H. Zhong, R. Fu, D. Wu, *Nat. Commun.* **2015**, *6*, 7221.
[17] J. Kossmann, R. Rothe, T. Heil, M. Antonietti, N. López-Salas, *J. Colloid Interface Sci.* **2021**, *602*, 880–888.
[18] Y. Shao, S. Zhang, M. H. Engelhard, G. Li, G. Shao, Y. Wang, J. Liu, I. A. Aksay, Y. Lin, *J. Mater. Chem.* **2010**, *20*, 7491–7496.
[19] J. W. Larsen, M. Freund, K. Y. Kim, M. Sidovar, J. L. Stuart, *Carbon* **2000**, *38*, 655–661.
[20] S. Liu, L. Cui, Z. Peng, J. Wang, Y. Hu, A. Yu, H. Wang, P. Peng, F.-F. Li, *Nanoscale* **2018**, *10*, 21764–21771.
[21] C. Liao, B. Liu, Q. Chi, Z. Zhang, *ACS Appl. Mater. Interfaces* **2018**, *10*, 44421–44429.
[22] a) L. Gao, J. Zhuang, L. Nie, J. Zhang, Y. Zhang, N. Gu, T. Wang, J. Feng, D. Yang, S. Perrett, X. Yan, *Nat. Nanotechnol.* **2007**, *2*, 577–583; b) L. Jiao, J. Wu, H. Zhong, Y. Zhang, W. Xu, Y. Wu, Y. Chen, H. Yan, Q. Zhang, W. Gu, L. Gu, S. P. Beckman, L. Huang, C. Zhu, *ACS Catal.* **2020**, *10*, 6422–6429.
[23] a) K. Fan, J. Xi, L. Fan, P. Wang, C. Zhu, Y. Tang, X. Xu, M. Liang, B. Jiang, X. Yan, L. Gao, *Nat. Commun.* **2018**, *9*, 1440; b) S. Lin, Y. Zhang, W. Cao, X. Wang, L. Qin, M. Zhou, H. Wei, *Dalton Trans.* **2019**, *48*, 1993–1999.
[24] a) Y. Song, K. Qu, C. Zhao, J. Ren, X. Qu, *Adv. Mater.* **2010**, *22*, 2206–2210; b) Y. Hu, X. J. Gao, Y. Zhu, F. Muhammad, S. Tan, W. Cao, S. Lin, Z. Jin, X. Gao, H. Wei, *Chem. Mater.* **2018**, *30*, 6431–6439.
[25] S. Wu, G. Wen, J. Wang, J. Rong, B. Zong, R. Schlögl, D. S. Su, *Catal. Sci. Technol.* **2014**, *4*, 4183–4187.
[26] R. Zhao, X. Zhao, X. Gao, *Chemistry* **2015**, *21*, 960–964.
[27] E. Renard, A. Deratani, G. Volet, B. Sebille, *Eur. Polym. J.* **1997**, *33*, 49–57.
[28] R. R. Shaikh, S. Pornpraprom, V. D'Elia, *ACS Catal.* **2018**, *8*, 419–450.
[29] a) J. Guadalupe, A. M. Ray, E. M. Maya, B. Gómez-Lor, M. Iglesias, *Polym. Chem.* **2018**, *9*, 4585–4595; b) M. A. Isaacs, C. M. A. Parlett, N. Robinson, L. J. Durndell, J. C. Manayil, S. K. Beaumont, S. Jiang, N. S. Hondow, A. C. Lamb, D. Jampaiah, M. L. Johns, K. Wilson, A. F. Lee, *Nat. Catal.* **2020**, *3*, 921–931; c) E. Gianotti, U. Diaz, A. Velty, A. Corma, *Catal. Sci. Technol.* **2013**, *3*, 2677–2688; d) S. Rat, A. Chavez-Sanchez, M. Jerigová, D. Cruz, M. Antonietti, *ACS Appl. Polymer Mater.* **2021**, *3*, 2588–2597.

Manuscript received: August 8, 2022
Accepted manuscript online: October 27, 2022
Version of record online: December 2, 2022